Electronic Supplementary Material (ESI) for Journal of Materials Chemistry A.

SUPPLEMENTARY INFORMATION

Hydrophobized Poly(Heptazine Imide) for Highly Effective Photocatalytic Hydrogen Peroxide Production in a Biphasic Fatty Alcohol-Water System

Igor Krivtsov,[a, b]* Ashish Vazirani,[a] Dariusz Mitoraj,[a] Mohamed M. Elnagar,[a] Christof Neumann,[c] Andrey Turchanin,[c] Yolanda Patiño,[b] Salvador Ordóñez,[b] Robert Leiter,[d] Mika Lindén,[e] Ute Kaiser,[d] Radim Beranek[a]*

[a] Institute of Electrochemistry, Ulm University, Albert-Einstein-Allee 47, 89081 Ulm, Germany
Igor Krivtsov, Ashish Vazirani, Dariusz Mitoraj, Mohamed Elnagar, Radim Beranek

[b] Department of Chemical and Environmental Engineering, University of Oviedo, 33006 Oviedo, Spain
Igor Krivtsov, Yolanda Patiño, Salvador Ordóñez

[c] Institute of Physical Chemistry and Abbe Center of Photonics, Friedrich Schiller University Jena, Lessingstr. 10, 07743 Jena, Germany
Christof Neumann, Andrey Turchanin

[d] Electron Microscopy of Materials Science, Central Facility for Electron Microscopy, Ulm University, Albert-Einstein-Allee 11, 89081, Ulm, Germany
Robert Leiter, Johannes Biskupek, Ute Kaiser

[e] Institute of Inorganic Chemistry II, Ulm University, Albert-Einstein-Allee 11, 89081, Ulm, Germany

*Corresponding authors: Igor Krivtsov (krivtsovigor@uniovi.es)
Radim Beranek (radim.beranek@uni-ulm.de)

1. Materials and Methods

1.1 Materials

Dicyandiamide (99%, Sigma Aldrich), potassium thiocyanate (KSCN) (98%, Merk), tetraethyl orthosilicate (TEOS) (99%, VWR), hydrochloric acid (HCl, 37 *wt*%, Merk), trichloro(hexyl)silane (HTS) (97%, Sigma Aldrich), trichloro(octadecyl)silane (OTS) (90%, Sigma Aldrich) and 1,1,1,3,3,3-hexamethyldisilazane (HMDS) (98.5%, Merk) were used to synthesize and hydrophobize PHI. Toluene (99.5%, VWR) and ethanol absolute (96%, VWR) were used as solvents during the modification of the photocatalysts. 1-butanol (99%, VWR), 1-octanol (99%, Merk), hydrogen peroxide (30 wt%, Sigma Aldrich), titanium oxysulfate sulfuric acid hydrate ($TiOSO_4$ nH_2O) (Synthesis grade, Sigma Aldrich), caprylic acid (98%, Sigma Aldrich), octyloctanoate (98%, Sigma Aldrich), hexachloroplatinic acid (H_2PtCl_6) (38 wt% Pt basis, Sigma Aldrich) were used for carrying out photocatalytic reactions and for the identification and quantification of the reaction products.

1.2 Synthesis

For the synthesis of potassium poly(heptazine imide) (KPHI), a modified procedure reported by Lotsch *et al.*[1] was used.

Melon polymer preparation was accomplished by self-condensation of dicyandiamide in a muffle furnace at 550 °C for 4 h. The obtained yellow solid was ground, washed 4 times with deionized water by centrifugation and dried in an oven at 70 °C for 24 h.

For the **KPHI** synthesis, 1.5 g of **melon polymer** and 3 g of KSCN were separately dried at 140 °C for 24 h, then the powders were ground together in a mortar, put in a lid-covered ceramic crucible and heated in a muffle furnace at a rate of 30 °C min^{-1} first to 400 °C for 1 h and then to 500 °C for 30 min. Thus, prepared KPHI samples were cooled down to room temperature and then thoroughly washed with deionized water by centrifugation for 5 times. The washed powders were dried at 70 °C for 24 h.

Silica-modified KPHI material (**KPHI-Si**) was prepared by adopting the procedure for the sol-gel fabrication of silica fibers reported by Sakka[2]. To 1 g of finely ground KPHI in a round bottom flask, 65 mL of ethanol was added and the suspension was sonicated for 1 h. After sonication, 37 mL of TEOS, 3 mL of H_2O and 0.15 mL of hydrochloric acid (37 wt %) were added to the mixture under vigorous stirring in this sequence. The sample was continuously stirred for 24 h, after which it was kept in a water bath at 50 °C for the next 24 h to induce silica polycondensation. In the next

step, the sample was thoroughly washed by centrifugation at 9000 rpm for 10 min first with water and then with ethanol. Then, the sample was dried in an oven at 70 °C for a few hours, ground in a mortar and dried at 110 °C overnight before undergoing hydrophobization.

The hydrophobization of KPHI-Si was performed according to the procedure developed by Resasco et al. for the hydrophobization of zeolites and oxides.[3, 4] For this, 1 g of KPHI-Si was taken into a 20 mL vial and to that 18.5 mL of toluene was added. After adding toluene, 1.5 mL of a hydrophobic agent being HTS (**KPHI-Si-HTS**), OTS (**KPHI-Si-OTS**) or HMDS (**KPHI-Si-HMDS**) was introduced to the same mixture and the vial was closed and stirred overnight at 50°C. The hydrophobized samples were washed three times with toluene (about 10 mL of solution each time) by centrifugation at 9000 rpm for 10 min. After the washing, the solid was dried at 70°C overnight to evaporate the excess toluene and then the temperature was increased to 110°C for the complete drying of the material.

For hydrogen evolution tests, 3 wt% of Pt was photodeposited on the KPHI samples. For this, 100 mg of the PHI photocatalyst was suspended in 20 mL of 50 % ethanol in a water mixture containing the required amount of H_2PtCl_6, the suspension was flushed with N_2 and irradiated with a 406 nm LED with the irradiance of 7.1 mW cm^{-2}. The solids were recovered by centrifugation at 9000 rpm, washed three times with deionized water and dried at 70 °C overnight.

1.3 Characterization

The surface morphology, elemental composition and elemental mapping of the synthesized materials were investigated using a ZEISS LEO 1550 VP scanning electron microscope (SEM) operating at an acceleration voltage of 10 kV equipped with an energy dispersive phonon (EDX) apparatus (INCA 400, Oxford Instruments, United Kingdom). To introduce the samples for the SEM study, a few milligrams (mg) of the materials were dispersed into 1.0 mL of ethanol through sonication for 5 min. Then, a thin film of each sample was prepared by drop casting a few microliters of the suspended samples onto titanium foil, as a conductive substrate, followed by drying at room temperature. Ti foil was selected to avoid the possible signal interference that can arise from Si or C-based substrates since these elements were present in the synthesized materials. After drying, a layer of Pt was sputtered onto the sample

surface to increase the conductivity, consequently, achieving a higher resolution. The thickness of the sputtered Pt layer was 20 nm.

The TGA measurements were performed from the powdered samples using a Netzsch TG 209 F1 analyzer. The TGA curves were registered at a heating rate of 10°C min^{-1} in air atmosphere. The DTG curves were obtained by numerical differentiation of the TGA data. XRD patterns were obtained using a Pananalytical X'pert PRO diffractometer equipped with a Pixel detector and operating at Cu Kα radiation. FTIR spectra were recorded by means of a Shimadzu IRTracer-100 spectrometer at a resolution of 4 cm^{-1} from the samples powdered and pressed into KBr pellets.

Nitrogen physisorption at 77 K was performed in a Quantachrome QuadraSorb apparatus. Prior to the measurements the samples were degassed at 140 °C for 22 h. The data was processed using QuadraWin software.

The ImageJ software was used for the contact angle analysis of the hydrophobized catalyst. For this, 0.03 g of each sample was suspended in 0.3 mL of ethanol, the suspension was sonicated for 40 min and then deposited on FTO slides by the doctor-blade method. A drop of water was put on the surface of the prepared films and the photograph was taken. The contact angle measurement plugin was used to process the images in ImageJ software.

In order to perform X-ray photoelectron spectroscopy (XPS), the powdered samples were placed on top of a conductive Au-substrate and fixed to the XPS sample holder. The measurements were performed using a UHV Multiprobe system (Scienta Omicron, Germany) with a monochromatic X-ray source (Al Kα) and an electron analyzer (Argus CU) with 0.6 eV energy resolution. Charge compensation during data acquisition was realized by an electron flood gun (NEK 150, Staib, Germany) at 6 eV and 50 μA. The background was subtracted and spectra were calibrated using the C1s peak (284.6 eV) before undergoing fitting using Voigt functions (30:70).

Diffuse-reflectance UV-vis spectra of solids were acquired by a Shimadzu UV-2600 UV-vis spectrophotometer from the samples mixed with $BaSO_4$.

High-resolution TEM analysis was performed using the Cc/Cs-corrected SALVE TEM operated at an accelerating voltage of 80kV. STEM- and spectral imaging using energy-dispersive x-ray spectroscopy (EDX) was performed using a ThermoFisher Talos at acceleration voltages of 80 kV and 120 kV. The samples were suspended in ethanol and drop-casted onto copper TEM support grids with holey carbon film.

1.4 Photocatalytic H_2O_2 production

Photocatalytic activity of the prepared samples was tested in visible-light assisted H_2O_2 production using alkyl alcohols (ethanol, 1-butanol and a model fatty alcohol 1-octanol) as electron donors. The mixtures of 5 mL of water and 5 mL of alcohols with suspended optimal photocatalysts loading under continuous stirring were irradiated with the 4.2 mW cm^{-2} LED 406 nm light source (***Note:*** *in case of using 1-butanol and 1-octanol as electron donors, a biphasic system was formed and the photocatalyst concentration is given per volume of either aqueous or organic phases it was suspended in*). Some selected reactions were also carried out under 365 LED irradiation (4.2 mW cm^{-2}) or under simulated sunlight (~100 mW cm^{-2}) using an Ushio 150 W Xe lamp in a light-condensing lamp housing (LOT-Oriel GmbH). The temperature of 20 °C in the photocatalytic reactors was maintained by a water-cooling jacket. Before irradiation started the suspensions were flushed with pure O_2 and sealed with rubber septa. This procedure was repeated each time after taking the samples out from the reactors for analysis. The samples of 0.1 mL (diluted if necessary, as to fit on the linear range of the calibration curve) were taken at certain time intervals, mixed with 2.4 mL of H_2O and 0.5 mL of $TiOSO_4 \bullet H_2SO_4$ solution to produce the yellow-coloured titanium peroxocomplex (***Note:*** *in case of using 1-butanol and 1-octanol as electron donors the samples were taken only from the bottom aqueous layer of the biphasic system*). H_2O_2 concentration was estimated by measuring the absorbance of the titanium peroxocomplex solutions at 420 nm using a Cary 60 (Agilent Technologies) spectrophotometer. The calibration curve was built using known concentrations of H_2O_2. The effect of acid concentration on the photocatalytic hydrogen peroxide production was evaluated by using 0.1 mol L^{-1}, 0.5 mol L^{-1}, 1.0 mol L^{-1} and 2.0 mol L^{-1} HCl solutions as an aqueous phase in the biphasic systems

The apparent quantum yield (AQY) of hydrogen peroxide production was estimated considering the two-electron oxygen reduction to H_2O_2 according to the reactions (1, 2).

$$C_8H_{17}\text{-}OH + 2h^+ \rightarrow C_8H_{16}O + 2H^+ \quad (1)$$

$$O_2 + 2H^+ + 2e^- \rightarrow H_2O_2 \quad (2)$$

The number of incident photons per second was determined by the formula:

$$\Phi = \frac{\mathrm{I}}{qE},$$

where ***I*** is the light power emitted by the LED (W), ***q*** is the charge of electron (C) and ***E*** is the energy of irradiation (eV). As the light power was measured by placing the sensor of the light meter directly on the LED window completely covering it, we assumed that all the emitted light would reach the reactor vessel placed in the water-cooling jacket positioned on the LED setup. Note that such an assumption has probably led to the underestimation of the AQY values.

The quantum yield was determined as:

$$\mathrm{AQY} = \frac{2\ \mathrm{n}H_2O_2\ N_A}{\Phi t} * 100\%,$$

where ***n***(H_2O_2) is the number of moles of H_2O_2 produced after 1 h or 24 h of irradiation, N_A is the Avogadro number and ***t*** is the irradiation time in s.

The different products obtained in the result of the photocatalytic oxidation of 1-octanol were analyzed by GC in a Shimadzu GC-2010 equipped with a FID detector, using a CP-Sil 8 CB (30 m x 0.25 mm x 0.25 µm) capillary column. For this, 1 mL of the sample was injected with a split ratio of 50. The injection port and the detector temperatures were kept at 250 °C and 300 °C respectively. The initial column temperature of 33 °C was kept for 0.5 min and increased to 99 °C with a rate of 10 °C/min. Then, the temperature was elevated to 205 °C at 5 °C/min and held for one minute. Finally, the column was heated to 230 °C at a rate of 10 °C/min and the temperature was maintained for 1 min. The assignment of the peaks on the chromatogram was carried out by comparing them to the chromatograms of commercially available standards.

The hydrogen evolution tests were performed using a 7.1 mW cm^{-2} LED 406 nm light source from equivolume 1-octanol/water biphasic mixture. The hydrogen was detected and quantified by a Shimadzu Tracera BID-2010 chromatograph by continuous sampling with 7 min time interval between measurements using online He-flushed (5 mL min^{-1}) system.

2. Results

2.1 Materials Characterization

Note on XPS characterization.

The low intensity of Si 2p peak on the spectra registered for the hydrophobized samples and the Si 2p signal of KPHI-OTS below the detection limit is explained by the low relative sensitivity factor of Si 2p (0.82) and the deposition of a shell of alkylsilanes reducing the Si signal further. The latter effect is especially accentuated in the case of the sample modified with OTS, which possesses the longest alkyl chain of all used hydrophobic agents (Figure S2). Moreover, one can observe that there is a small signal in the region of Si 2p appearing in the spectrum of the parent KPHI sample (**Figure S2a**). However, the intensity of the signal is much lower than registered for the KPHI-Si, KPHI-HTS and KPHI-HMDS samples (**Figure S2**). Therefore, we attribute its presence to possible contamination of the parent material with Si coming from glassware, considering that during the handling of the synthesized KPHI material (washing, centrifugation) its alkaline suspension might have interacted with glassware, causing dissolution of some SiO_2.

The K $2p_{3/2}$ signal can in principle be found between 293 - 295 eV depending on the chemical surrounding (**Figure S3**). It appears at 293.1, 292.7 and 292.5 eV for the KPHI, KPHI-Si and KPHI-OTS samples, respectively. However, in the spectrum of KPHI-HTS, this peak is significantly shifted to 295.8 eV (**Figure S3**), which we ascribe to charging effects (see below). Apart from the potassium in KPHI, this signal is attributed to the potassium of the KCl crystals, whose presence was confirmed by the STEM-EDX technique (see **Figure S9**). Also, the presence of another peak at 292.1 eV in the spectrum of KPHI-HTS draws attention (**Figure S3**). As during the measurement, the charge was compensated using electrons with ~ 6 eV, this different potential could lead to a shift of 6 eV from 285/286 eV (C-C/C-O) to 292 eV, explaining the appearance of this maximum.

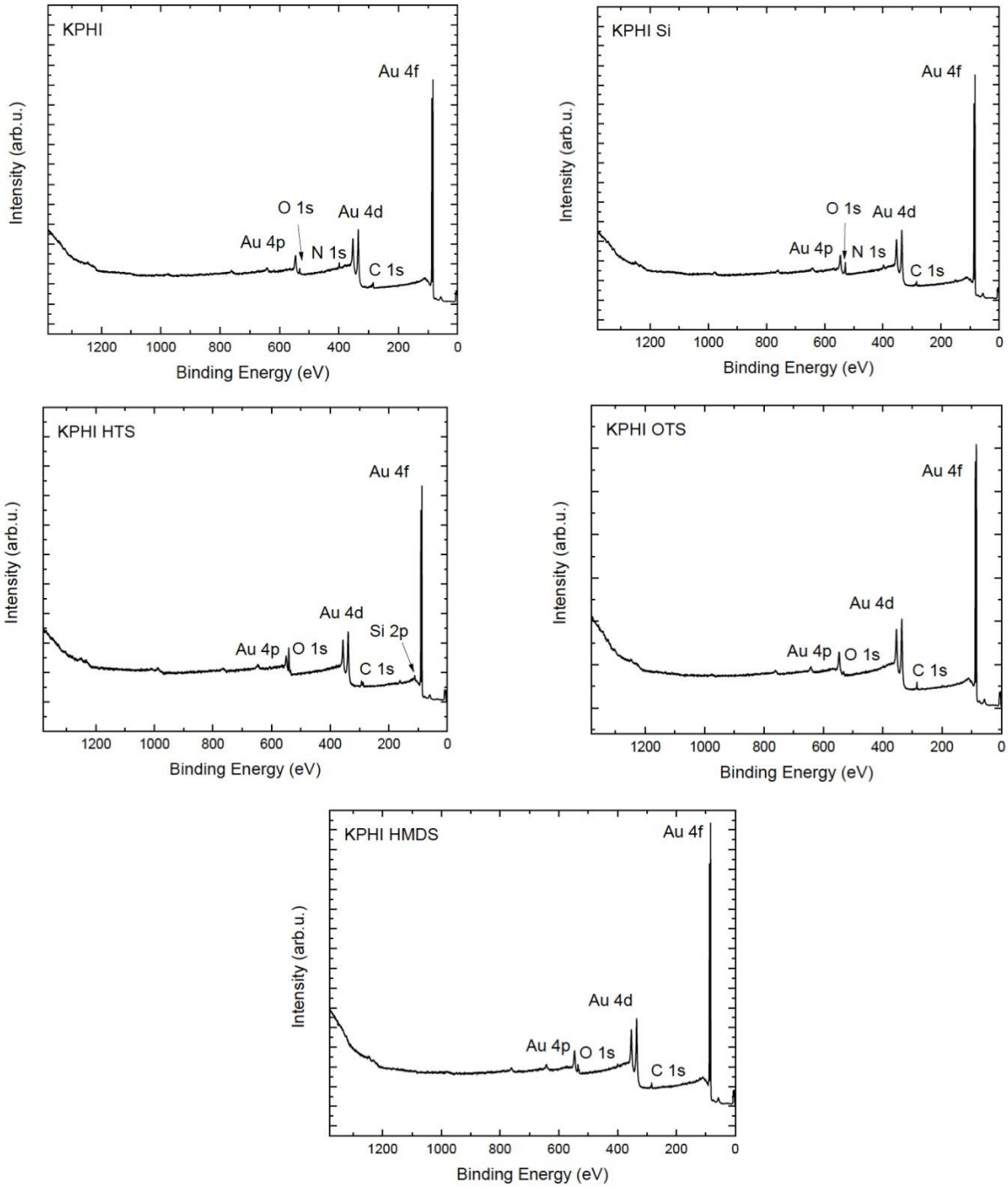

Figure S1. Survey XP spectra of the prepared photocatalysts.

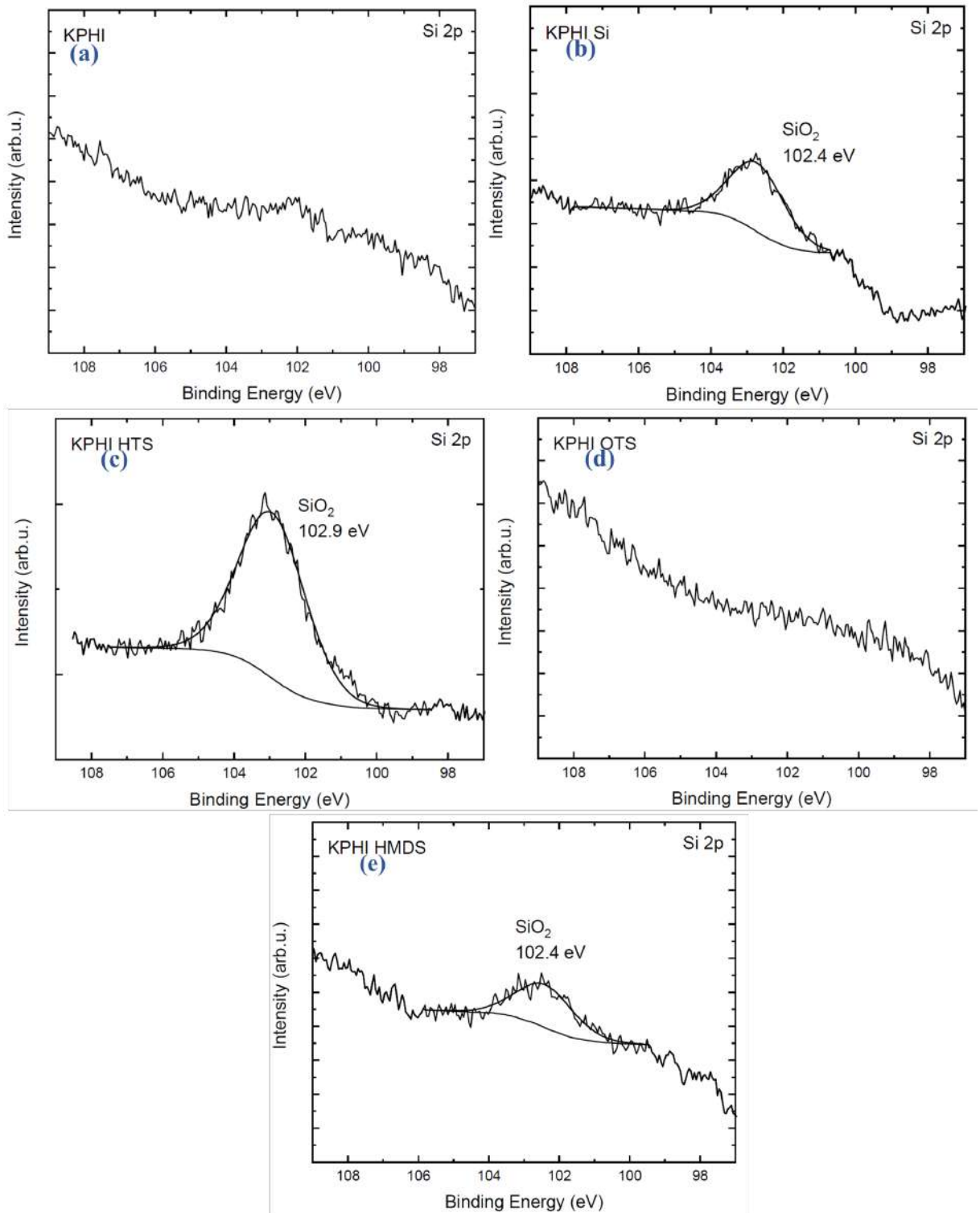

Figure S2. Si2p XP spectra obtained for the (a) KPHI, (b) KPHI-Si, (c) KPHI-HTS, (d) KPHI-OTSand (e) KPHI-HMDS samples.

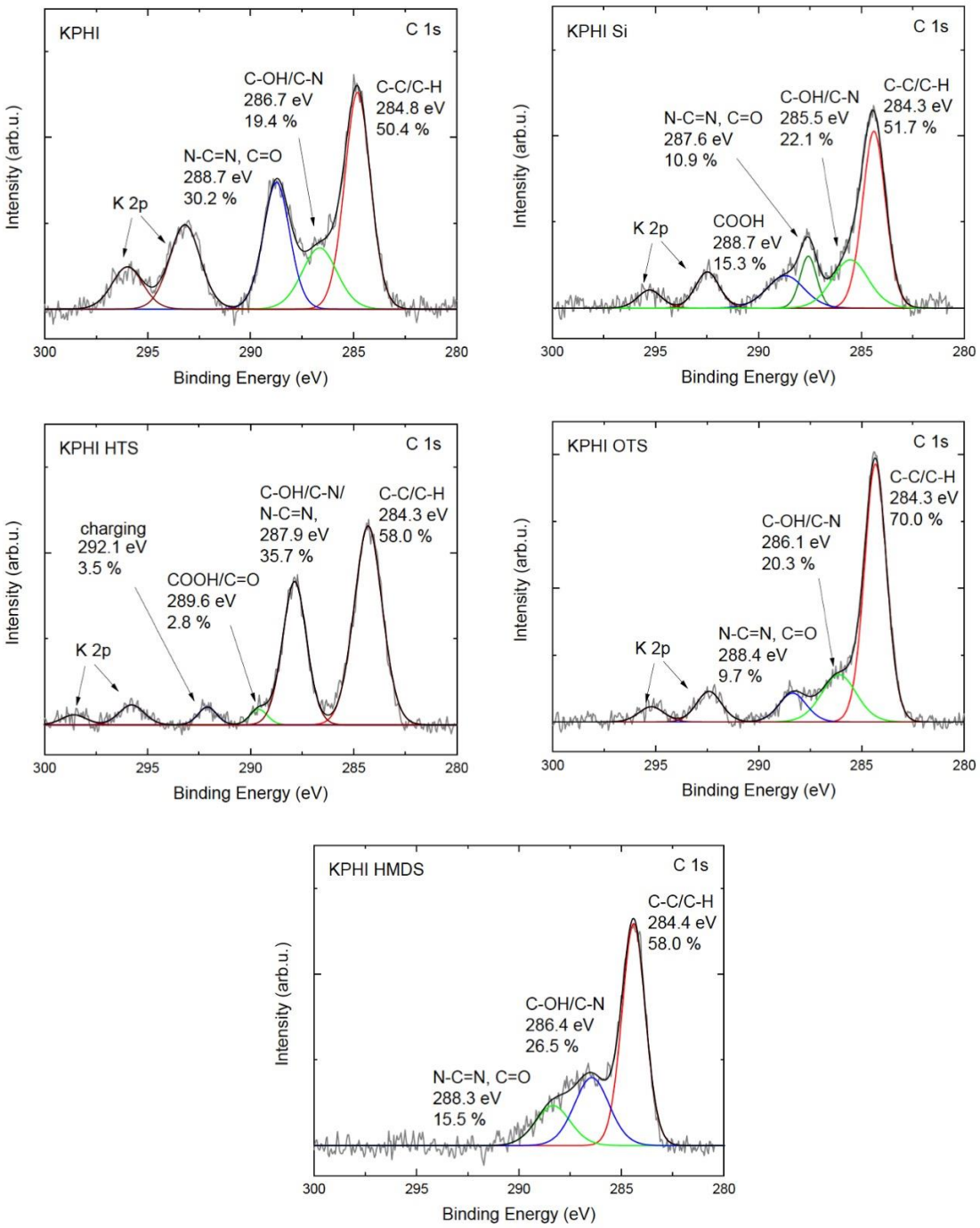

Figure S3. C1s XP spectra obtained for the (a) KPHI, (b) KPHI-Si, (c) KPHI-HTS, (d) KPHI-OTS and (e) KPHI-HMDS samples.

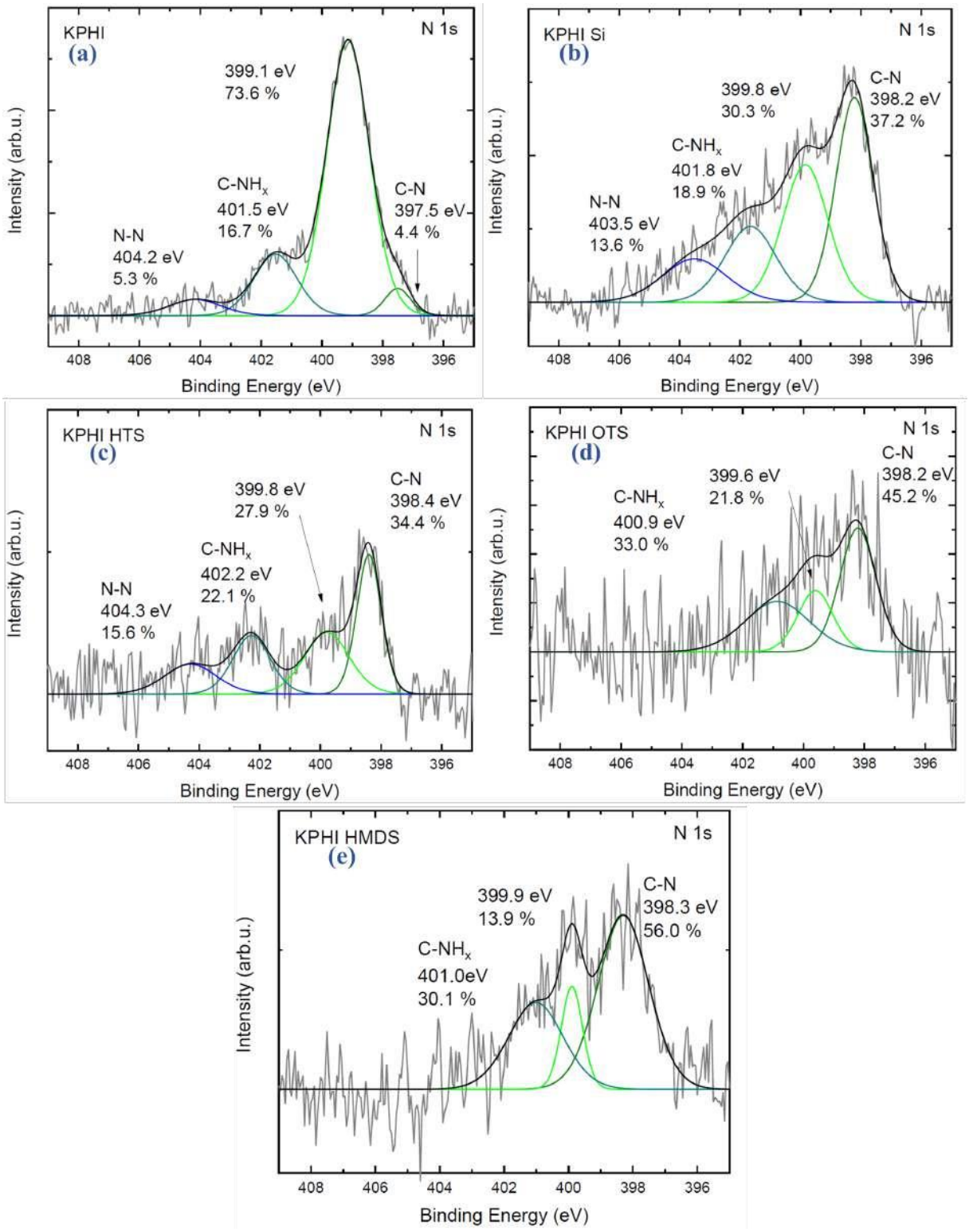

Figure S4. N1s XP spectra obtained for the KPHI, KPHI-Si, KPHI-HTS, KPHI-OTS and KPHI-HMDS samples.

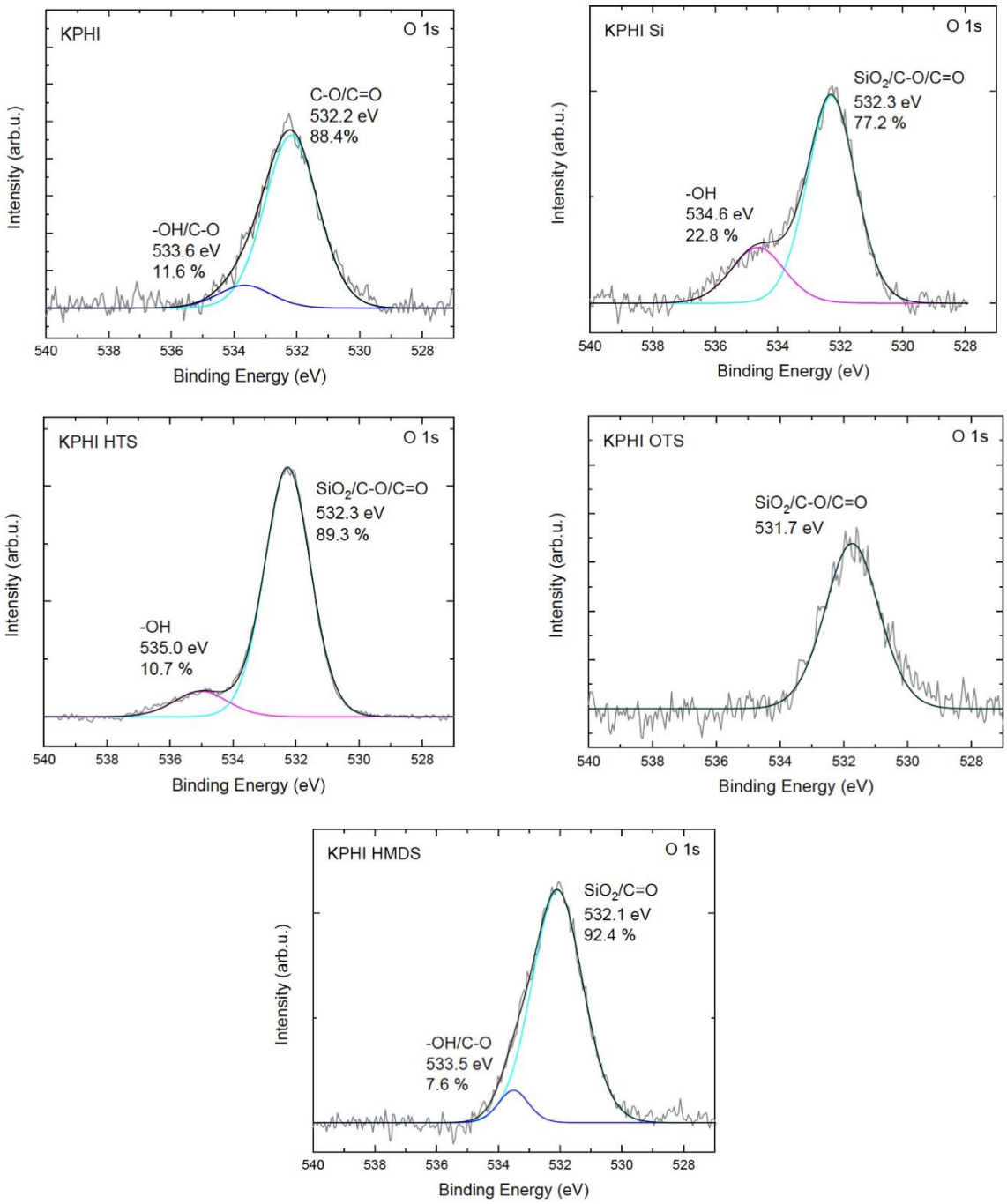

Figure S5. O1s XP spectra obtained for the KPHI, KPHI-Si, KPHI-HTS, KPHI-OTS and KPHI-HMDS samples.

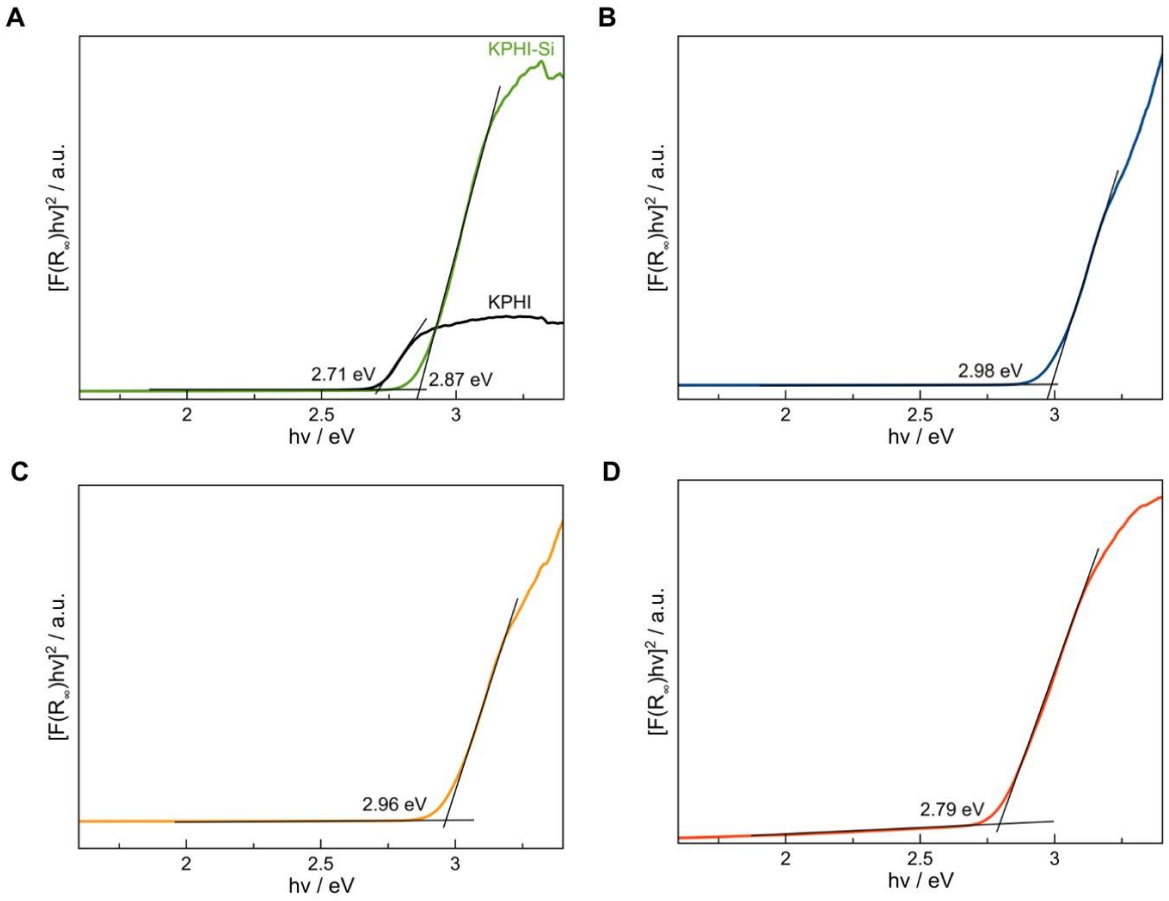

Figure S6. **Materials characterization.** Diffuse reflectance UV-vis spectra of the a) hydrophilic KPHI and KPHI-Si, b) KPHI-HTS, c) KPHI-OTS and d) KPHI-HMDS samples transformed using the Tauc formalism for the determination of absorption edges (assuming the direct nature of the transition).

Note on SEM characterization. Figure S7 displays the SEM micrographs of KPHI compared to the Si-modified KPHI before and after silylation with different hydrophobic agents including HTS, OTS, and HMDS. A rough surface characterized by agglomerated irregular and dense particles is observed for the KPHI, as shown in Figure S7a. In contrast, the Si-modified KPHI (KPHI-Si) exhibits a rougher surface morphology with dispersed small fragmented particles (Figure S7b), which possibly explains the higher surface area of this material. Remarkably, the silylation of KPHI-Si with HTS hardly changes its surface morphology and roughness since the surface of KPHI-HTS is still rough with dispersed small fragmented particles, as observed in Figure S7c. This indicates that the silylation of KPHI-Si with short alkyl chain precursors does not alter its surface morphology. On the other hand, the surface roughness of KPHI-Si is significantly decreased after the silylation of KPHI-Si with OTS

(KPHI-OTS) as observed by the lower density of the small fragmented particles over the surface (Figure S7d). The decrease in surface roughness of KPHI-OTS might be due to the long alkyl chain of OTS. Moreover, the particles are slightly more agglomerated after the silylation of KPHI-Si with HDMS (KPHI-HDMS), as observed in Figure S7e. Based on these observations, the surface area of KPHI-Si is expected to substantially decrease after the silylation with OTS compared to that with HTS or HDMS. The SEM-EDX elemental mapping analysis indicates that Si is homogeneously distributed over the surfaces of the Si-modified materials, confirming their homogeneity. Furthermore, the EDX elemental composition analysis evidences the reduction of potassium concentration upon the sol-gel modification and hydrophobization procedures (Figure S8).

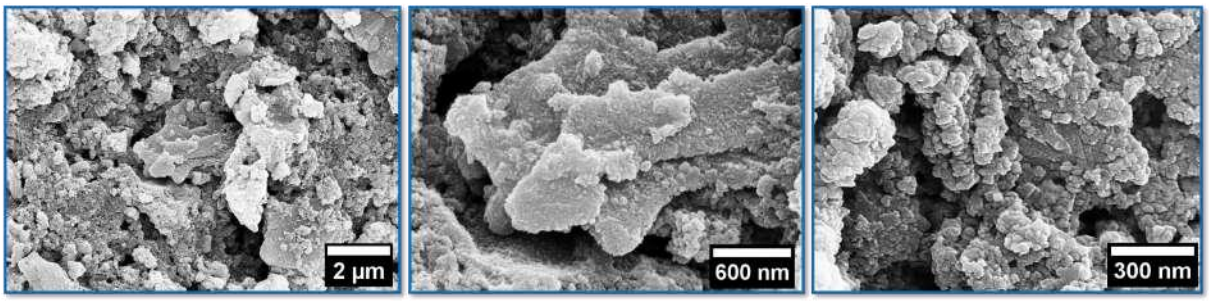

(a) KPHI

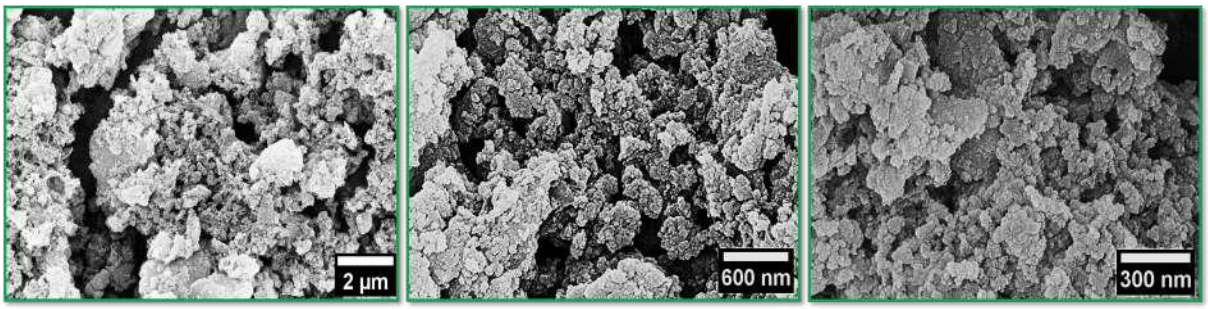

(b) KPHI-Si

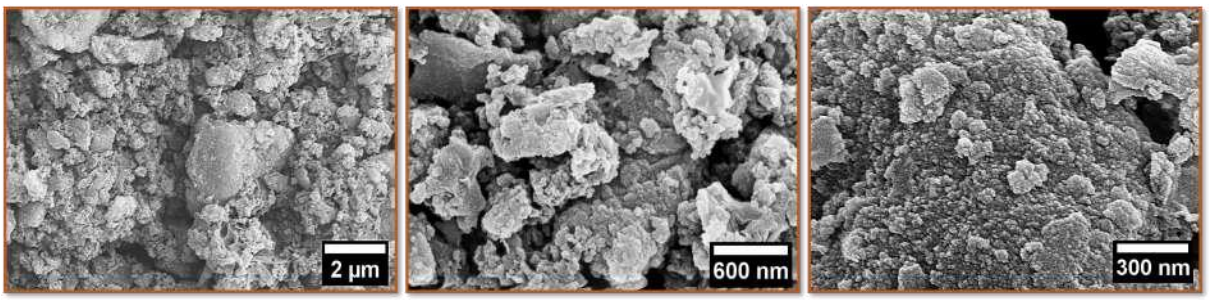

(c) KPHI-HTS

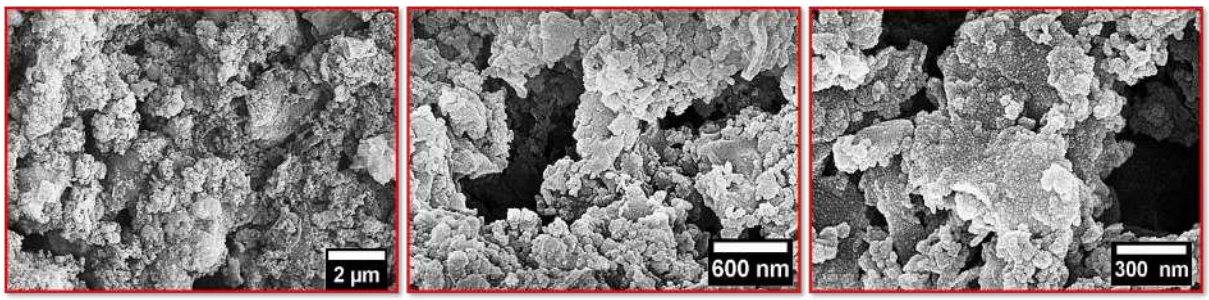

(d) KPHI-OTS

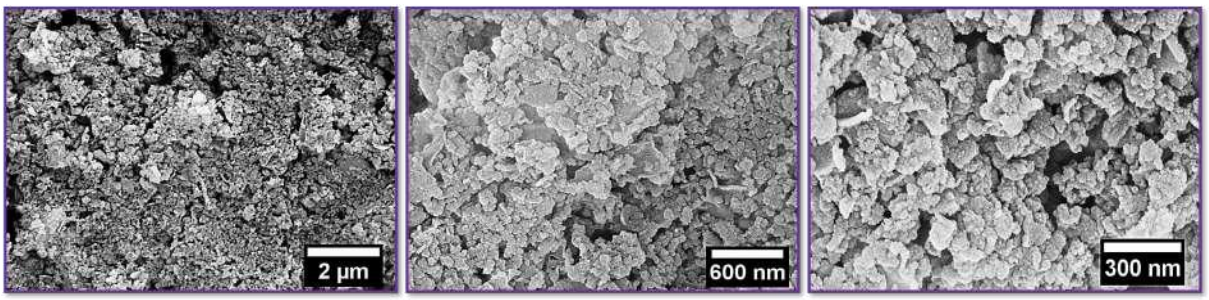

(e) KPHI-HDMS

Figure S7: SEM images of the synthesized KPHI(a-c), KPHI-Si(d-f), KPHI-HTS(g-i),KPHI-OTS(j-l), and KPHI-HMDS(m-o) samples.

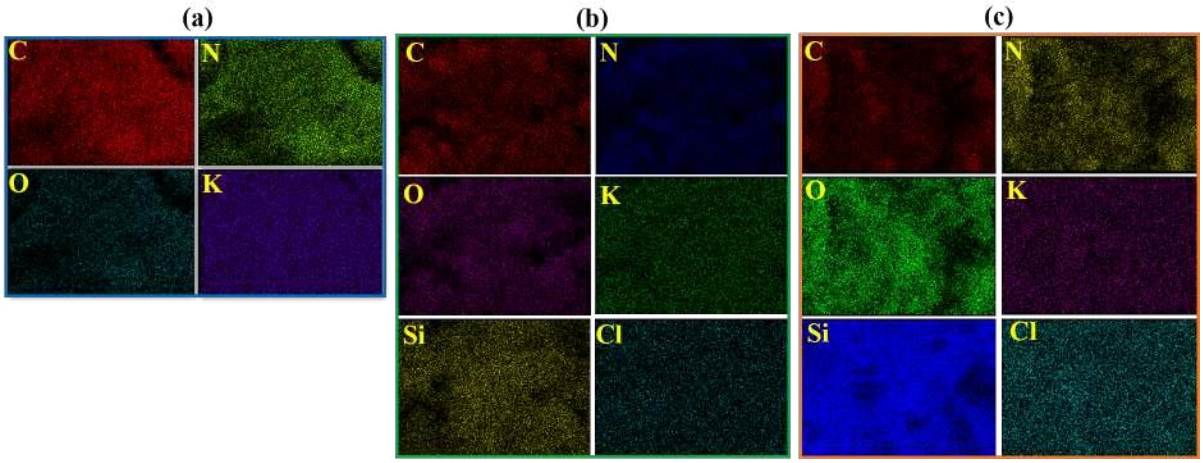

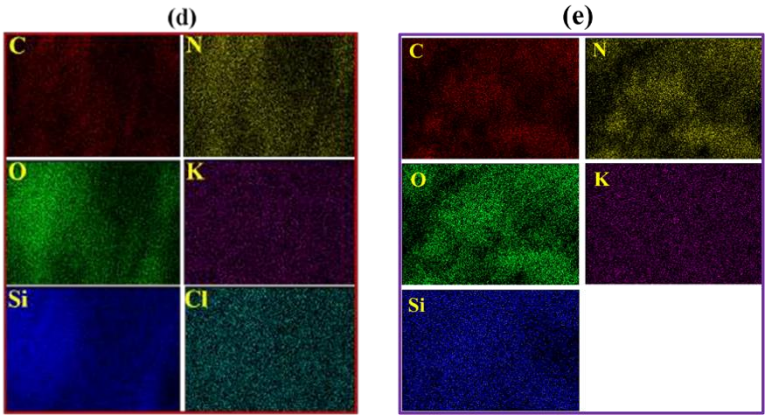

Figure S8. S E M - E D X mapping images of the synthesized samples: (a) KPHI, (b) KPHI-Si, and (c) KPHI- HTS, (d) KPHI-OTS and (e) KPHI-HMDS.

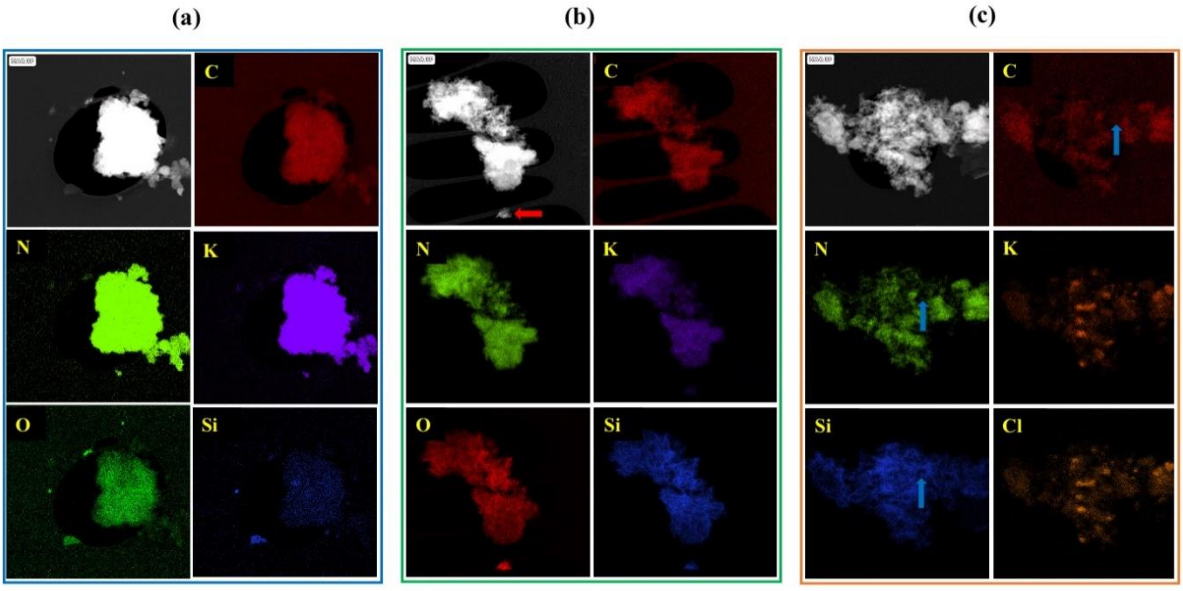

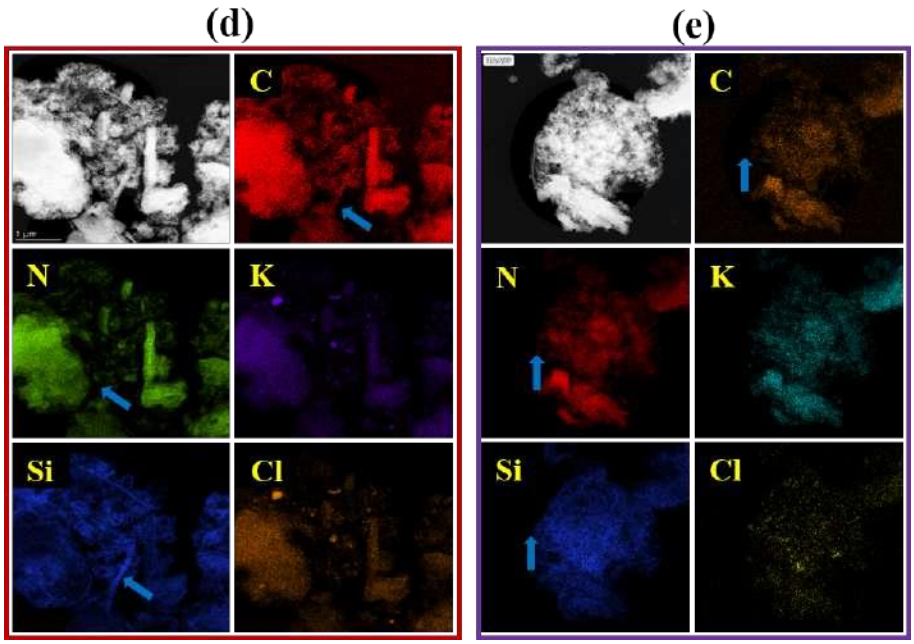

Figure S9. High-angle annular dark field (HAADF) STEM images (top left image in each panel) and corresponding EDX elemental mapping of the synthesized samples (a) KPHI, (b) KPHI-Si, (c)KPHI-HTS, (d) KPHI-OTS and (e) KPHI-HMDS.

Table S1. Surface elemental composition of the synthesized materials determined by XPS and EDX bulk elemental analysis (TEM and SEM)

Sample	Surface elemental composition (at %) by XPS analysis						Elemental composition (at %) by TEM-EDX analysis**						Elemental composition (at %) by SEM-EDX analysis**						Surface:bulk ratio*					
	C	N	O	K	Cl	Si	C	N	O	K	Cl	Si	C	N	O	K	Cl	Si	C	N	O	K	Cl	Si
KPHI	55.7	25.1	14.6	4.6	0.0	0.0	41.7	43.5	3.3	11.6	0.0	0.0	26.6	61.6	1.6	10.2	0.0	0.0	2.1	0.4	9.1	0.5	/	/
KPHI-Si	37.9	21.3	27.0	2.54	1.7	12.1	30.9	43.8	14.7	2.54	0.5	7.5	23.8	40.1	21.2	3.67	0.4	10.8	1.6	0.5	1.3	0.7	4.3	1.1
KPHI-HTS	31.6	3.9	35.6	0.7	2.0	26.2	22.6	26.7	31.7	2.4	2.4	14.3	29.8	34.1	21.4	2.1	2.3	10.3	1.1	0.1	1.7	0.3	0.9	2.5
KPHI-OTS	71.3	4.2	12.9	2.7	8.7	0.0	26.0	20.3	32.0	1.7	1.7	28.3	15.3	21.2	35.5	2.3	2.5	23.2	4.7	0.2	0.4	1.2	3.5	/
KPHI-HMDS	46.6	9.3	33.4	0.0	0.0	10.7	21.5	34.5	27.0	2.1	0.0	14.8	10.1	35.2	32.9	3.9	0.0	17.8	4.6	0.3	1.0	-	-	0.6

*The surface to bulk ratio was calculated using XPS and SEM-EDX analyses, respectively

** The discrepancy in TEM-EDX and SEM-EDX results is likely to be attributed to a smaller analysis area, while using the TEM technique.

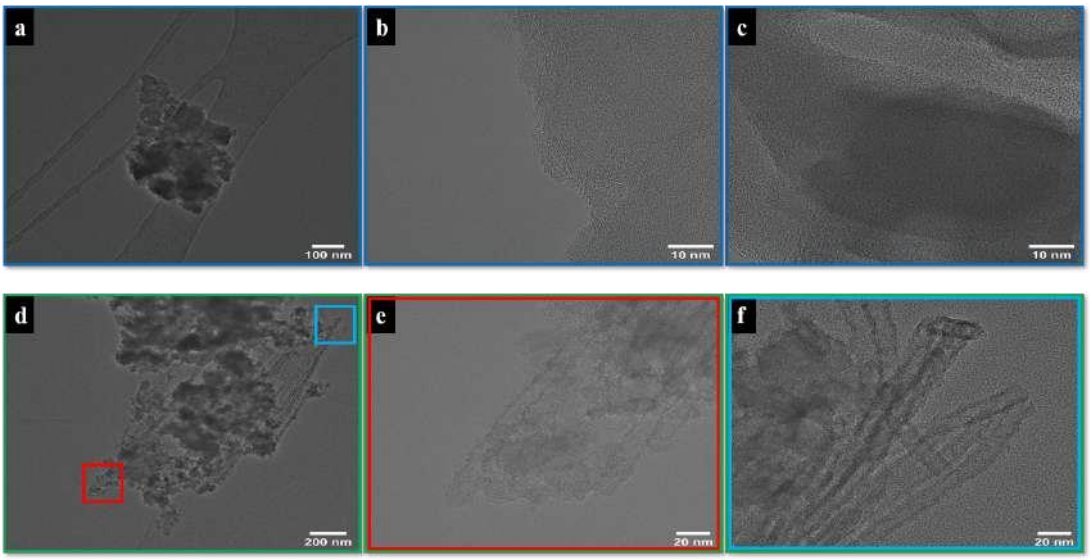

Figure S10. HRTEM images of the KPHI (a-c) and KPHI-Si (d-f) samples.

2.2 Photocatalytic Hydrogen Peroxide Production

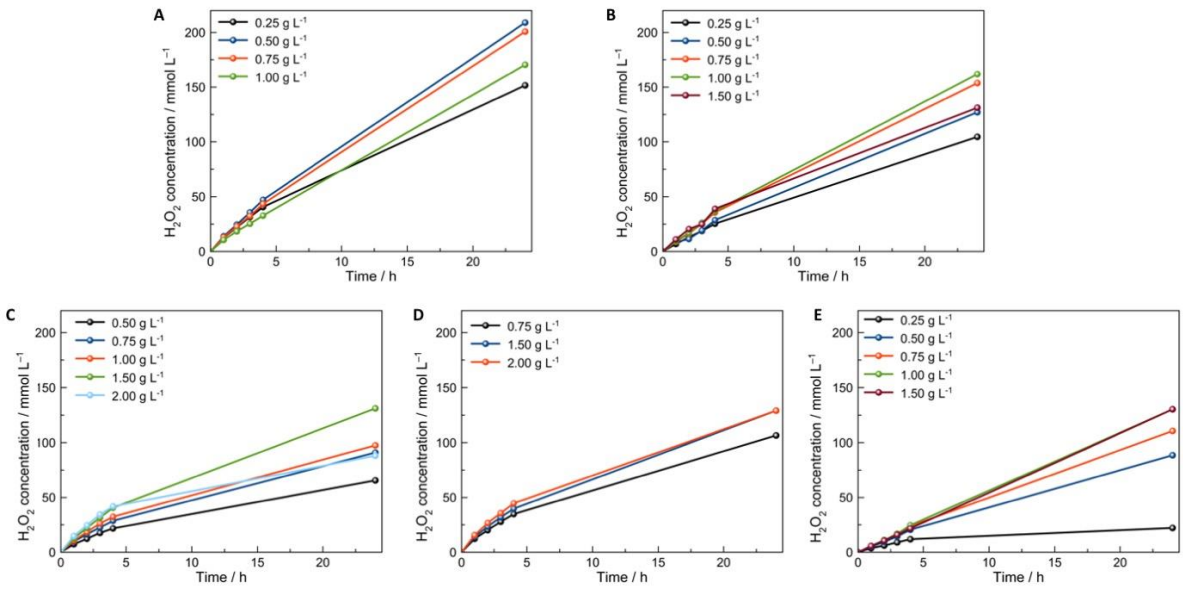

Figure S11. Photocatalytic tests. Photocatalytic production of H_2O_2 using ethanol as an electron donor in presence of various concentrations of (a) KPHI, (b) KPHI-Si, (c) KPHI-HTS, (d) KPHI-OTS and (e) KPHI-HMDS. Conditions: 5mL ethanol, 5 mL H_2O, pH 6.5–7.0, LED 406 nm (4.2 mW cm^{-2}), 22 °C, O_2 1 atm. The suspensions were saturated with pure O_2 before irradiation and after each sampling.

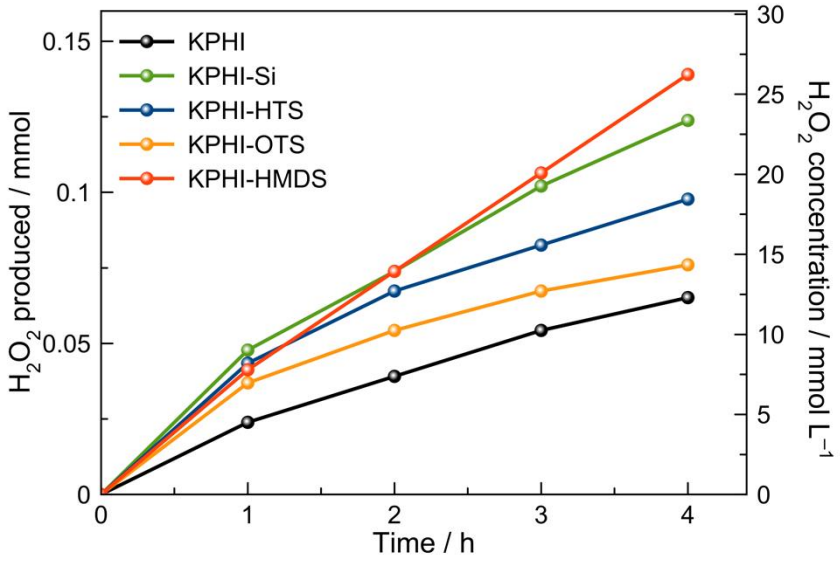

Figure S12. Photocatalytic tests. Photocatalytic production of H_2O_2 in biphasic system using 1-butanol as an electron donor in presence of (a) KPHI, (b) KPHI-Si, (c) KPHI-HTS, (d) KPHI-OTS and (e) KPHI-HMDS. Conditions: 5mL 1-butanol, 5 mL H_2O, pH 6.5–7.0, LED 406 nm (4.2 mW cm^{-2}), 22 °C, O_2 1 atm. The photocatalyst concentrations are 0.5 g L^{-1} for KPHI, 1.0 g L^{-1} for KPHI-Si and KPHI-HMDS and 1.5 g L^{-1} for KPHI-HTS and KPHI-OTS. The suspensions were saturated with pure O_2 before irradiation and after each sampling.

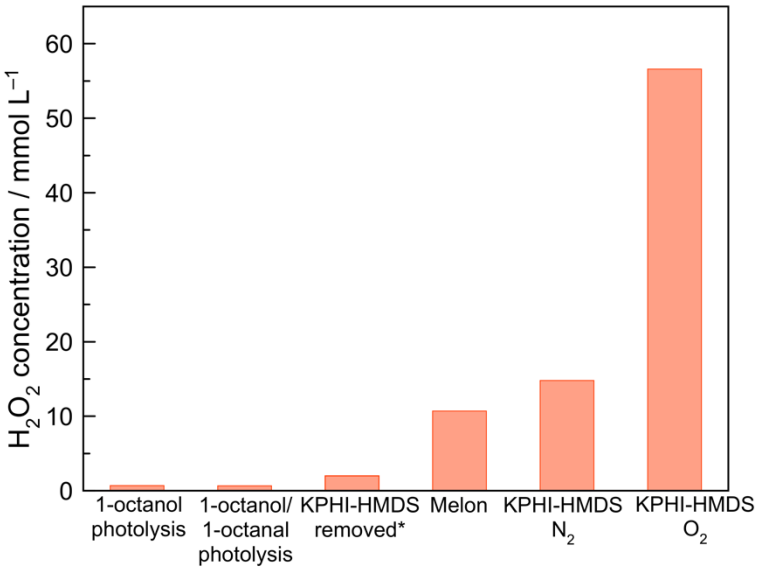

Figure S13. Photocatalytic tests. Control experiments for photocatalytic production of H_2O_2 in biphasic system using 1-octanol as an electron donor. Conditions: 5 mL 1-octanol (or mixture of 1-octanol and 2% v/v 1-octanal), 5 mL 0.5 mol L^{-1} HCl, LED 406 nm (4.2 mW cm^{-2}), 22 °C, O_2 1 atm, 24 h.

*The KPHI-HMDS photocatalyst was removed by filtration after 72 h of irradiation and the biphasic mixture was irradiated for 24 h, after which the surplus of produced H_2O_2 concentration was estimated.

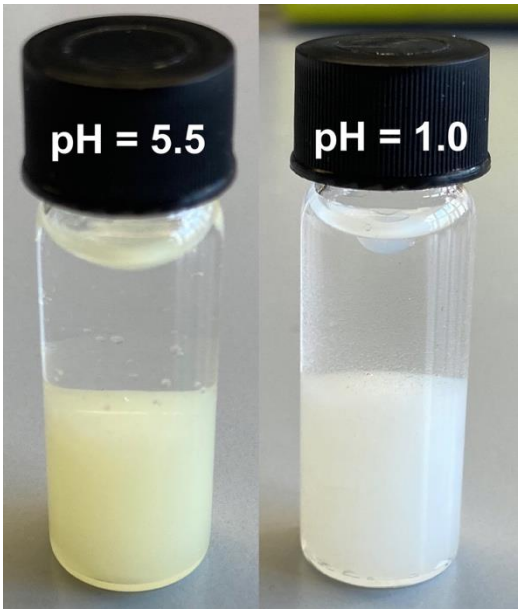

Figure S14. Photocatalytic tests. Photographs of biphasic systems composed of 5 mL benzyl alcohol (bottom layer) and 5 mL of H_2O with the suspended KPHI-HMDS photocatalyst.

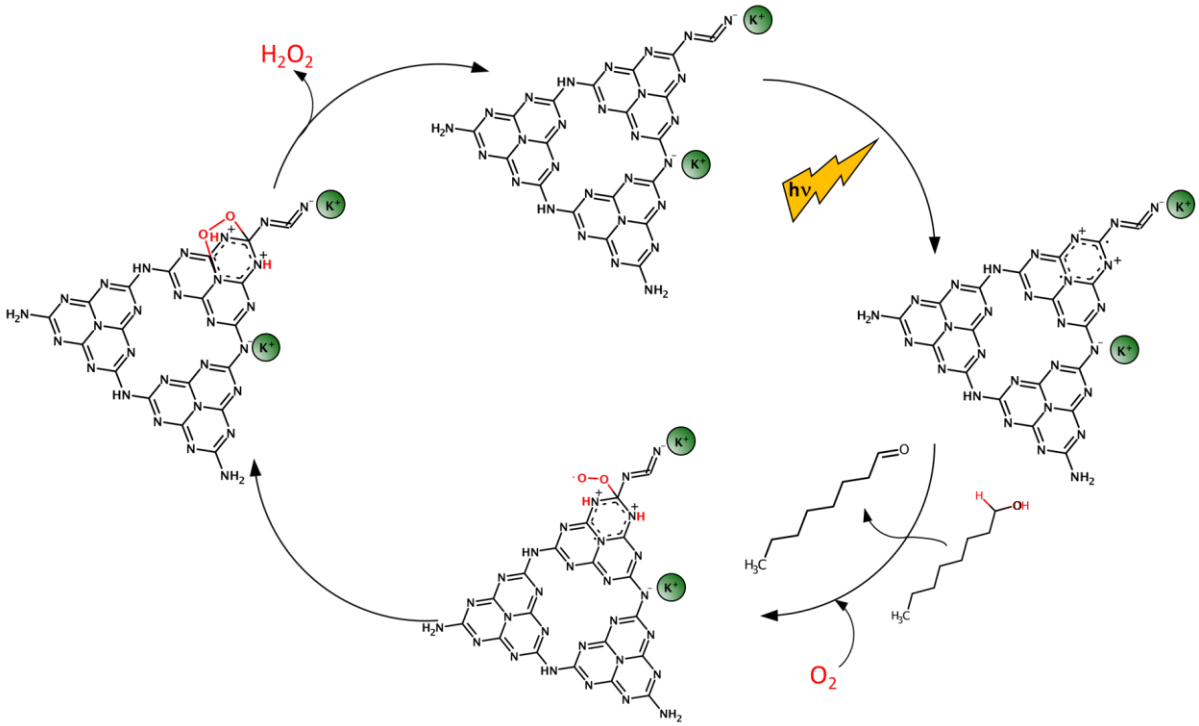

Figure S15. Photocatalytic mechanism. Proposed mechanism of photocatalytic H_2O_2 production over K-PHI photocatalyst using 1-octanol as an electron donor; the key mechanistic steps (protonation of the heptazine nitrogen sites and formation of the intermediate PHI-bound endoperoxide species) are adapted from the scheme for H_2O_2 production at conventional (non-ionic) carbon nitride reported by Shiraishi *et al*.[5]

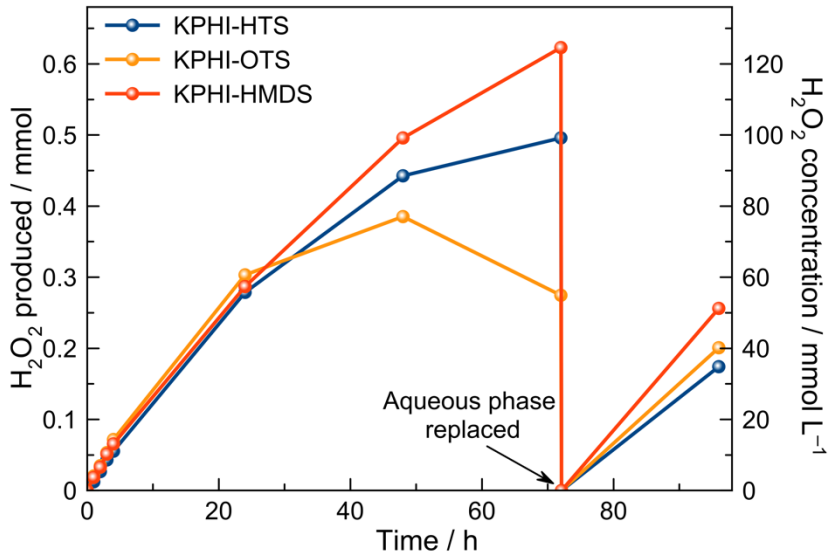

Figure S16. Photocatalytic tests. Photocatalytic production of H_2O_2 in biphasic system using 1-octanol as an electron donor. Conditions: 5 mL 1-octanol, 5 mL 0.5 mol L^{-1} HCl, LED 406 nm (4.2 mW cm^{-2}), 22 °C, O_2 1 atm. The photocatalyst concentrations are 1.0 g L^{-1} for KPHI-HMDS and 1.5 g L^{-1} for KPHI-HTS and KPHI-OTS. The suspensions were saturated with pure O_2 before irradiation and after each sampling.

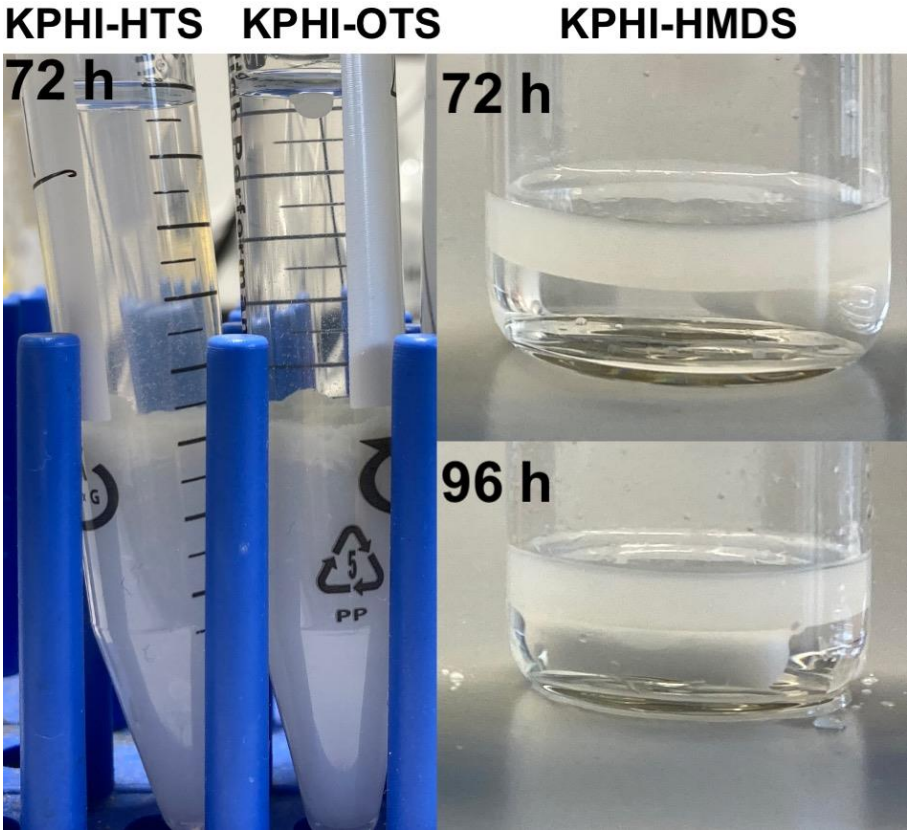

Figure S17. Photocatalytic tests. Photographs of biphasic systems composed of 5 mL 1-octanol and 5 mL 0.5 mol L^{-1} HCl with suspended photocatalysts after irradiation with LED 406 nm (4.2 mW cm^{-2}), 22 °C, O_2 1 atm.

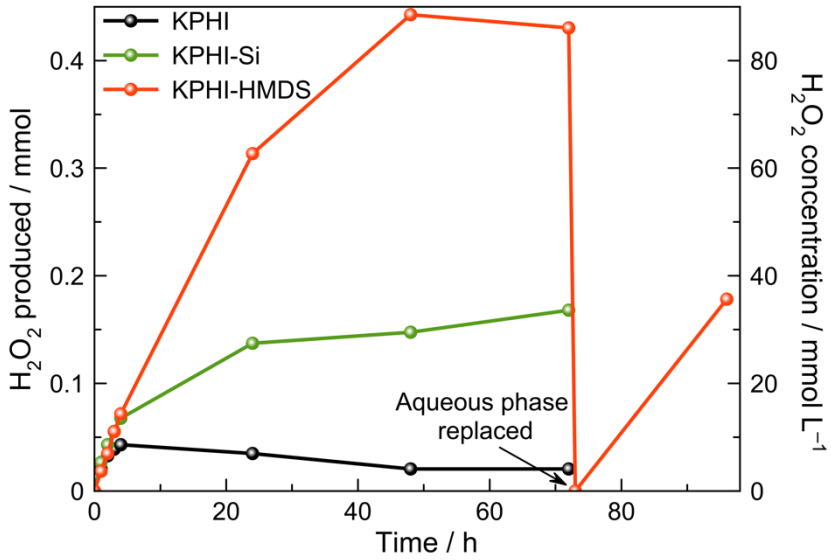

Figure S18. Photocatalytic tests. Photocatalytic production of H_2O_2 in biphasic system using 1-octanol as an electron donor. Conditions: 5 mL 1-octanol, 5 mL 1.0 mol L^{-1} HCl, LED 406 nm (4.2 mW cm^{-2}), 22 °C, O_2 1 atm. The photocatalyst concentrations are 0.5 g L^{-1} for KPHI, 1.0 g L^{-1} for KPHI-Si and KPHI-HMDS. The suspensions were saturated with pure O_2 before irradiation and after each sampling.

Figure S19. Photocatalytic tests. Photographs of biphasic system composed of 5 mL 1-octanol and 5 mL 1.0 mol L^{-1} HCl with suspended HMDS photocatalyst after irradiation for 72 h with LED 406 nm (4.2 mW cm^{-2}), 22 °C, O_2 1 atm.

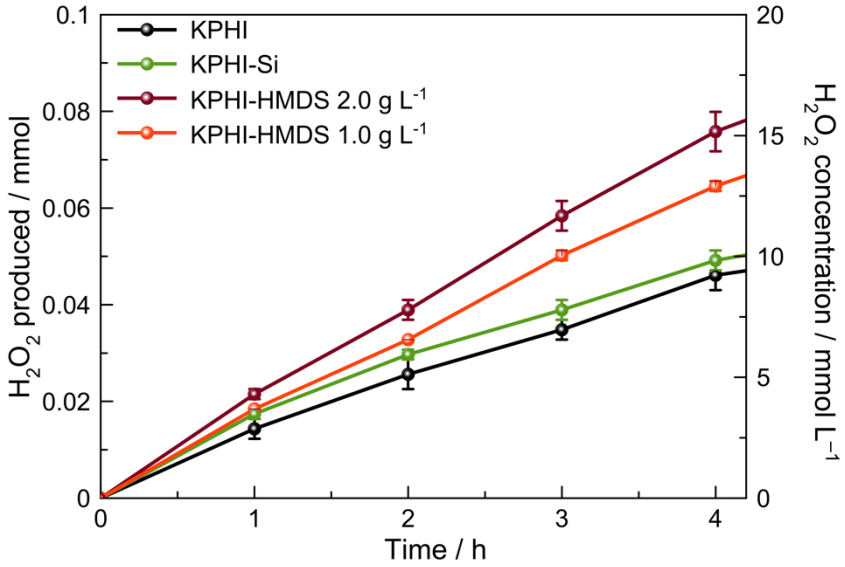

Figure S20. Photocatalytic tests. Photocatalytic production of H_2O_2 in biphasic system using 1-octanol as electron donor. Conditions: 5 mL 1-octanol, 5 mL 0.5 mol L^{-1} HCl, LED 406 nm (4.2 mW cm^{-2}), 22 °C, O_2 1 atm. The photocatalyst concentrations are 0.5 g L^{-1} for KPHI, 1.0 g L^{-1} for KPHI-Si and 1.0 and 2.0 g L^{-1} for KPHI-HMDS. The suspensions were saturated with pure O_2 before irradiation and after each sampling.

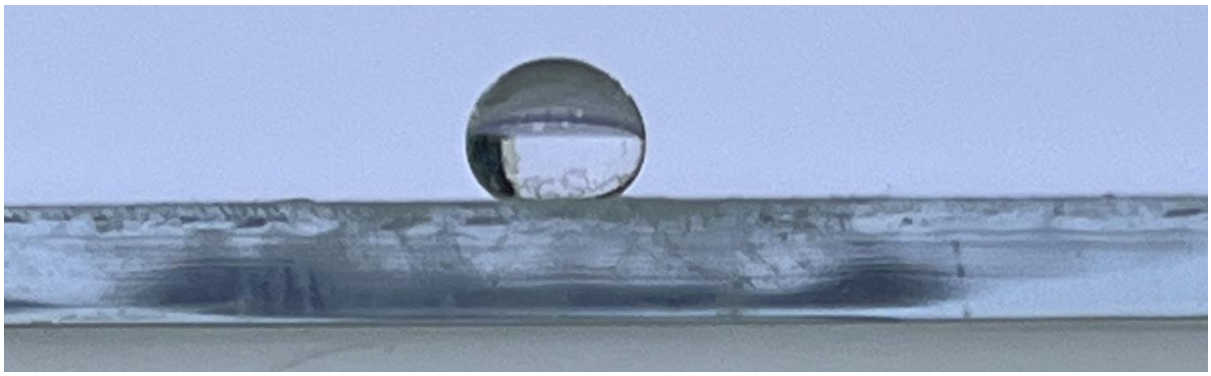

Figure S21. Photograph of the doctor-bladed film prepared from KPHI-HMDS photocatalyst recover after 24 h of irradiation in 1-octanol/water (0.5 mol L^{-1} HCl) biphasic system.

Table S2. Pseudo-first-order rate constants calculated for production of H_2O_2 in biphasic system using 1-octanol as an electron donor. Conditions: 5 mL 1-octanol, 5 mL 0.5 mol L^{-1} HCl, LED 406 nm (4.2 mW cm^{-2}), 22 °C, O_2 1 atm. The rate constants were calculated on the basis of the data obtained during the first 4 h of irradiation. Using longer timeframe of the reaction did not allow to obtain a reasonable fit.

Sample	Rate constant / h^{-1}	R
KPHI	0.381	0.8895
KPHI-Si	0.338	0.8738
KPHI-HTS	0.499	0.8441
KPHI-OTS	0.418	0.9539
KPHI-HMDS 1.0 g L^{-1}	0.418	0.9126
KPHI-HMDS 2.0 g L^{-1}	0.418	0.9081

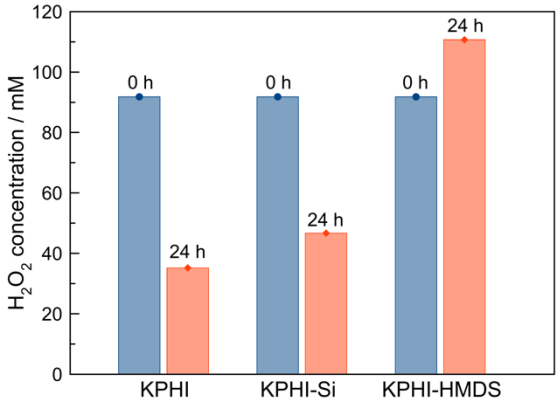

Figure S22. Photocatalytic tests. Photocatalytic production/decomposition of H_2O_2 in biphasic system using 1-octanol as an electron donor. Conditions: 5 mL 1-octanol, 5 mL 0.5 mol L^{-1} HCl and 91.8mM H_2O_2, LED 406 nm (4.2 mW cm^{-2}), 22 °C, O_2 1 atm. The photocatalyst concentrations are 0.5 g L^{-1} for KPHI, 1.0 g L^{-1} for KPHI-Si and KPHI-HMDS.

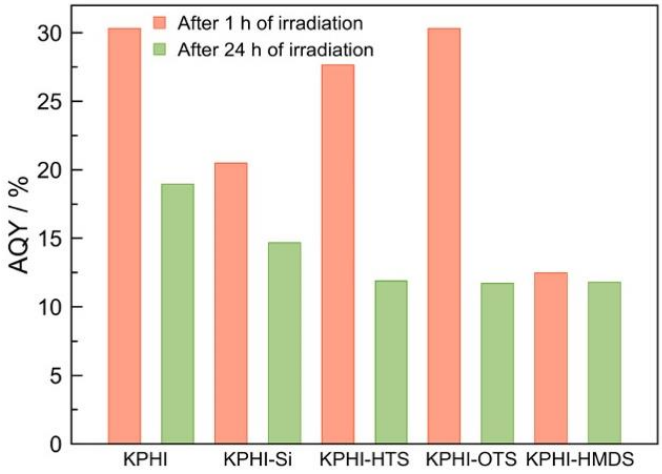

Figure S23. Apparent quantum yield. Apparent quantum yield of photocatalytic H_2O_2 production in monophasic equivolume ethanol/water mixture

Conditions: 5mL ethanol, 5 mL H_2O, pH 6.5–7.0, LED 406 nm (4.2 mWcm^{-2}), 22 °C, O_2 1 atm. The photocatalyst concentrations were 0.5 g L^{-1} for KPHI, 1.0 g L^{-1} for KPHI-Si and KPHI-HMDS and 1.5 g L^{-1} for KPHI-HTS and KPHI-OTS. The suspensions were saturated with pure O_2 before irradiation and after each sampling.

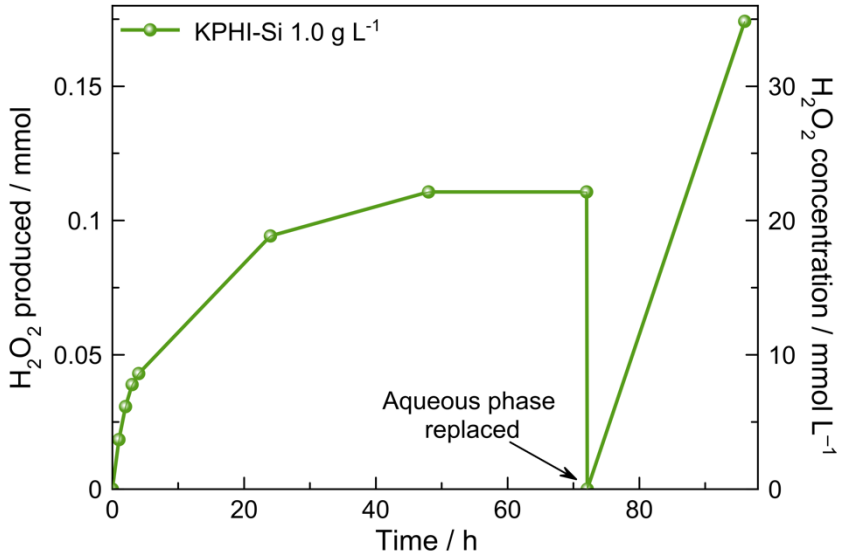

Figure S24. Photocatalytic tests. Photocatalytic production of H_2O_2 in biphasic system using 1-octanol as an electron donor. Conditions: 5 mL 1-octanol, 5 mL 0.5 mol L^{-1} HCl, LED 406 nm (4.2 mW cm^{-2}), 22 °C, O_2 1 atm. The suspensions were saturated with pure O_2 before irradiation and after each sampling.

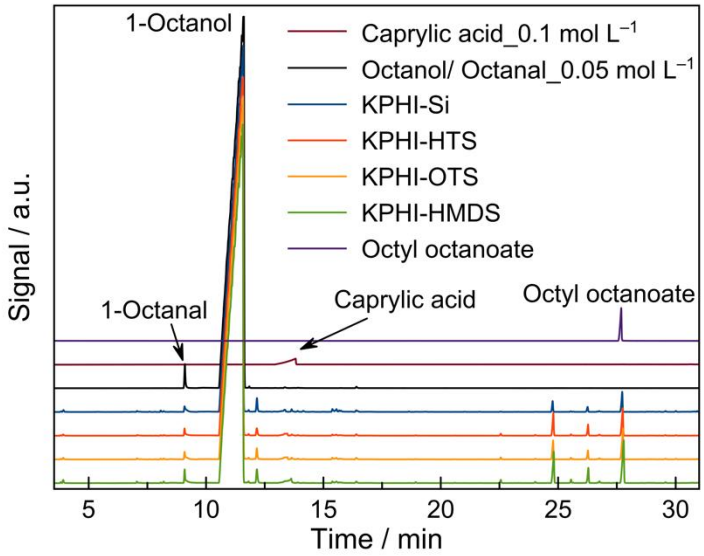

Figure S25. Chromatography. GC-FID chromatograms of the organic phases of the biphasic mixtures after 96 h of total irradiation. Conditions: 5 mL 1-octanol, 5 mL 0.5 mol L^{-1} HCl, LED 406 nm (4.2 mW cm^{-2}), 22 °C, O_2 1 atm. The photocatalyst concentrations are 0.5 g L^{-1} for KPHI, 1.0 g L^{-1} for KPHI-Si and KPHI-HMDS and 1.5 g L^{-1} for KPHI-HTS and KPHI-OTS. The suspensions were saturated with pure O_2.

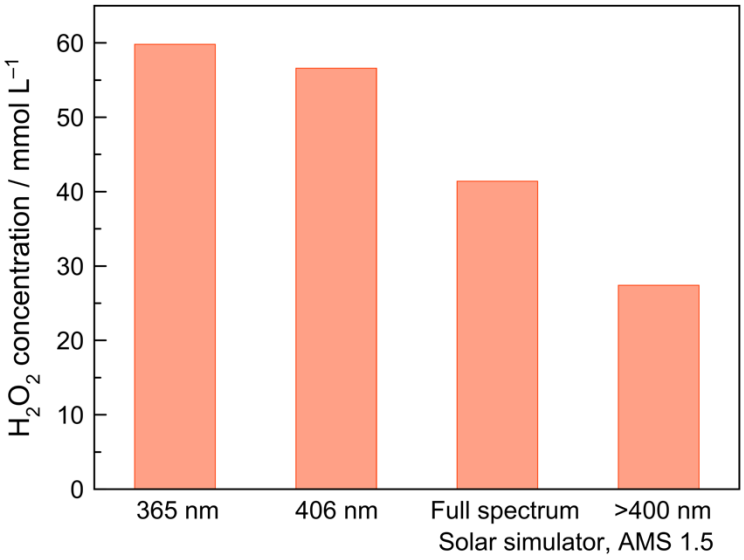

Figure S26. Photocatalytic tests. Photocatalytic production of H_2O_2 by KPHI-HMDS (1.0 g L^{-1}) in biphasic system using 1-octanol as an electron donor. Conditions: 5 mL 1-octanol, 5 mL 0.5 mol L^{-1} HCl, different irradiation sources, 22 °C, O_2 1 atm, 24 h. The suspensions were saturated with pure O_2 before irradiation and after sampling.

Table S3. Comparison of H_2O_2 production performance by different photocatalysts

Photocatalyst	Electron donor	Irradiation	H_2O_2 maximum concentration (mmol L^{-1})	H_2O_2 production rate (mmol h^{-1})	Ref.
Metal oxide photocatalysts					
TiO_2*	1-phenylethanol**	280–400 nm 13.8 mW cm^{-2}	40.2 (12 h)	0.017	[6]
Au–TiO_2*	ethanol	290–390 nm 3.9 mW cm^{-2}	14.0 (24 h)	0.12	[7]
AuAg–TiO_2*	ethanol	>280 nm	3.4 (12 h)	0.0014	[8]
Au–$BiVO_4$	H_2O	420 – 500 nm 2.69 mW cm^{-2}	0.04 (10 h)	0.00012	[9]
Polymeric carbon nitride-based materials					
g-C_3N_4*	ethanol	>420 nm	113 (36 h)	0.31	[10]
g-C_3N_4*	ethanol	>420 nm 2.69 mW cm^{-2}	6 (12 h)	0.025	[5]
Mesoporous g-C_3N_4*	ethanol	>420 nm 2.69 mW cm^{-2}	18 (24 h)	0.0038	[11]
PHI*	ethanol	Solar simulated light >400 nm AM 1.5G 175 mW cm^{-2}	146.8 (2 h)	0.55	[12]
PHI*	ethanol	>420 nm	4.0 (3 h)	-	[13]
PHI*	glycerol	Solar simulated light 100 mW cm^{-2}	17.5 (continuous flow reactor)	0.31	[14]

O-doped C_3N_4*	2-propanol	>420 nm 35.2 mW cm^{-2}	14.6	0.09	[15]
g-C_3N_4-PDI/BN	H_2O	(420–500 nm) 4.3 mW cm^{-2}	1.2	0.0015	[16]
Organic polymers					
Triazine-Acetylene COF*	ethanol	>420 nm	7.28 (1 h)	0.0182	[17]
(Diarylamino)benzene-Based COF*	ethanol	420-700 nm 0.546 mW cm^{-2}	1.92 (5 h)	0.0046	[18]
Piperazine-Linked Metalphthalocyanine Frameworks *	ethanol	>400 nm	0.210 (0.5 h)	0.01	[19]
s-triazine and pyrimidine condensation product	H_2O	>420 nm 350 mW cm^{-2}	0.32 (12 h)	0.001	[20]
1,3,5-triformylphloroglucinol (Tfp) and p-phenylenediamine (Pa)–based COF	H_2O	420-700 nm 40.8 mW cm^{-2}	425 (8 h)	0.53	[21]
Resorcinol–formaldehyde resins	H_2O	420-700 nm 14.03 mW cm^{-2}	3.3 (24 h)	0.0041	[22]
Biphasic systems					
Alkylated anthraquinones***	toluene	395 nm LED	118 (2 h)	0.49	[23]
MIL-125-NH2	benzyl alcohol**	>420 nm	16 (4 h)	0.008	[24]
Hydrophobic PHI****	1-octanol	406 nm 4.2 mW cm^{-2}	120 (72 h)	0.008	This work

*The photocatalyst, electron donor, H_2O_2 and other reaction products are in the same phase that complicates the separation of hydrogen peroxide for its further use.

**Benzylic alcohols that can autocatalyze H_2O_2 production are used as electron donors[25-27]

***Homogeneous photocatalysis. The photocatalyst is in the same phase as the organic reaction products, thus presenting difficulties for its separation.

****The photocatalyst can be filtered out from the organic phase.

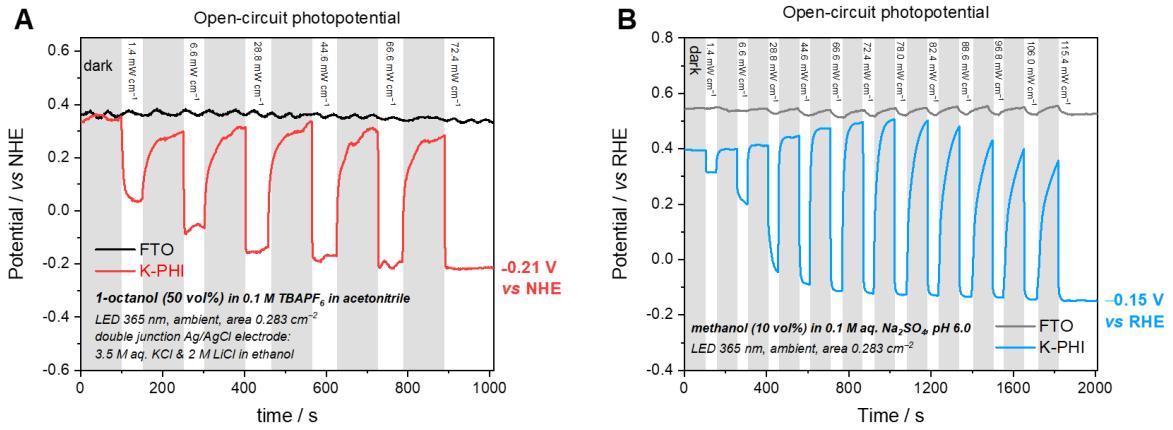

Figure S27. Open-circuit photopotential curves of K-PHI and of pristine FTO glass recorded under LED 365 nm irradiation of varied intensity in (A) acetonitrile solution of tetrabutylammonium hexafluorophosphate ($TBAPF_6$, 0.1 M) with 50 v/v% 1-octanol. The measured photopotential corresponds to the *quasi*-Fermi level (*i.e.*, electrochemical potential) of electrons ($^*E_{Fn}$) in the film. For comparison, measurements in an aqueous 0.1 M Na_2SO_4 (pH 6.0) electrolyte with 10 v/v% methanol are also shown in (B).

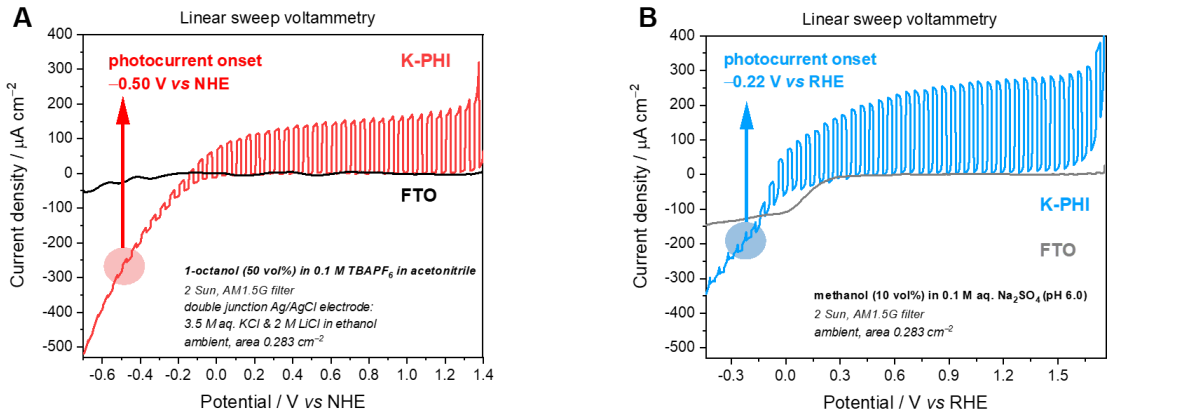

Figure S28. Linear sweep voltammetry of K-PHI and of pristine FTO glass in (A) acetonitrile solution of tetrabutylammonium hexafluorophosphate ($TBAPF_6$, 0.1 M) with 50 v/v% 1-octanol recorded under intermittent irradiation (2 sun, AM1.5G filter; 5 s/5s light on/off) with a sweep rate of 5 mV s^{-1} from the substrate side. For comparison, measurements carried out in an aqueous 0.1 M Na_2SO_4 (pH 6.0) electrolyte with 10 v/v% methanol are also shown in (B).

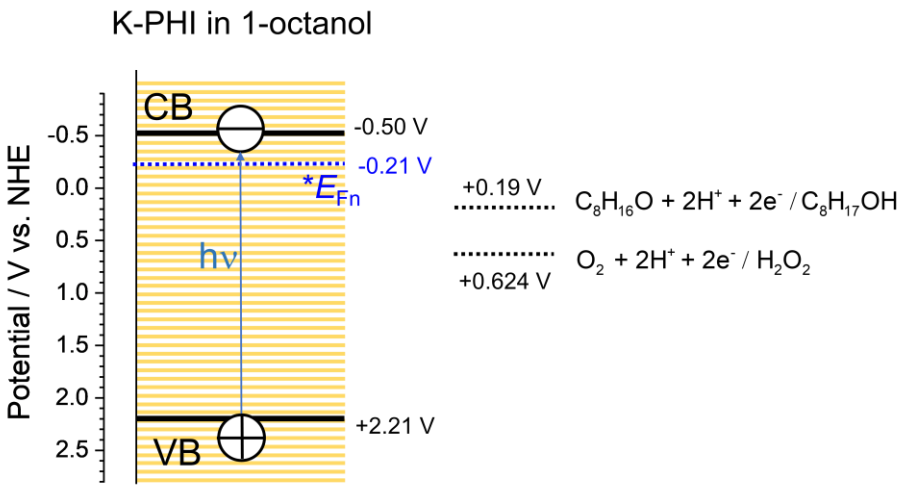

Figure S29. Simplified energy scheme of K-PHI in 1-octanol. The electrode potential of the conduction band edge (–0.50 V vs. NHE) was estimated from the photocurrent onset potential of the K-PHI electrode in 1-octanol containing electrolyte solution (Figure S28A). The *quasi*-Fermi level (*i.e.*, electrochemical potential) of electrons ($^*E_{Fn}$) under irradiation was determined from open-circuit photopotential measurements in 1-octanol containing electrolyte solution (Figure S27A). The equilibrium potentials for two-electron reduction of O_2 to H_2O_2 and oxidation of 1-octanol and 1-octanal are very rough estimates, as these values were calculated using the Gibbs free energies of formation (see below), whereby the differences of Gibbs free energies of reactants and products in 1-octanol were neglected, and no correction for equilibrium potential for the hydrogen evolution reaction was made since its value in 1-octanol has not been reported. Please note that the equilibrium potential for H_2O_2 formation from dioxygen (+0.624 V vs. NHE) is slightly different from the typically reported value (+0.695 V vs. NHE) which is calculated from the Gibbs free energy of formation of H_2O_2 *in an aqueous solution* (–134.1 kJ/mol).

$\Delta_f G^{\ominus}_{\text{1-octanol}} = -120.2\,\text{kJ/mol}$ Source: https://www.chemeo.com/cid/49-458-0/1-Octanol

$\Delta_f G^{\ominus}_{\text{1-octanal}} = -83.04\,\text{kJ/mol}$ Source: https://www.chemeo.com/cid/47-179-2/Octanal

$\Delta_f G^{\ominus}_{H_2O_2(l)} = -120.35\,\text{kJ/mol}$ Source: P. Atkins, J. de Paula, Atkins' Physical Chemistry, Oxford University Press, Oxford, 2014.

References

1. H. Schlomberg, J. Kroger, G. Savasci, M. W. Terban, S. Bette, I. Moudrakovski, V. Duppel, F. Podjaski, R. Siegel, J. Senker, R. E. Dinnebier, C. Ochsenfeld and B. V. Lotsch, *Chem. Mater.*, 2019, **31**, 7478-7486.
2. S. Sakka, in *Better Ceramics Through Chemistry*, eds. C. J. Brinker, D. E. Clark and D. R. Ulrich, North-Holland, New Yourk, 1984, p. 91.
3. P. A. Zapata, Y. Huang, M. A. Gonzalez-Borja and D. E. Resasco, *J. Catal.*, 2013, **308**, 82-97.
4. T. G. V. Erazo, *Surface Modification of TIO2 for Photocatalytic Selective Oxidation of Organic Compounds in Biphasic and Single Phase Systems. Master Thesis* https://shareok.org/handle/11244/47041. , University of Oklahoma, 2016.
5. Y. Shiraishi, S. Kanazawa, Y. Sugano, D. Tsukamoto, H. Sakamoto, S. Ichikawa and T. Hirai, *ACS Catal.*, 2014, **4**, 774-780.
6. Y. Shiraishi, S. Kanazawa, D. Tsukamoto, A. Shiro, Y. Sugano and T. Hirai, *ACS Catal.*, 2013, **3**, 2222-2227.
7. M. Teranishi, S.-i. Naya and H. Tada, *The Journal of Physical Chemistry C*, 2016, **120**, 1083-1088.
8. D. Tsukamoto, A. Shiro, Y. Shiraishi, Y. Sugano, S. Ichikawa, S. Tanaka and T. Hirai, *ACS Catal.*, 2012, **2**, 599-603.
9. H. Hirakawa, S. Shiota, Y. Shiraishi, H. Sakamoto, S. Ichikawa and T. Hirai, *ACS Catal.*, 2016, **6**, 4976-4982.
10. Z. Xu, Y. Li, Y. Cao, R. Du, Z. Bao, S. Zhang, F. Shao, W. Ji, J. Yang, G. Zhuang, S. Deng, Z. Wei, Z. Yao, X. Zhong and J. Wang, *J. Energ. Chem.*, 2022, **64**, 47-54.
11. Y. Shiraishi, Y. Kofuji, H. Sakamoto, S. Tanaka, S. Ichikawa and T. Hirai, *ACS Catal.*, 2015, **5**, 3058-3066.
12. P. Sharma, T. J. A. Slater, M. Sharma, M. Bowker and C. R. A. Catlow, *Chem. Mater.*, 2022, **34**, 5511-5521.
13. P. Zhang, Y. W. Tong, Y. Liu, J. J. M. Vequizo, H. W. Sun, C. Yang, A. Yamakata, F. T. Fan, W. Lin, X. C. Wang and W. Y. Choi, *Angew. Chem. Int. Ed.*, 2020, **59**, 16209-16217.
14. Y. B. Zhao, P. Zhang, Z. C. Yang, L. N. Li, J. Y. Gao, S. Chen, T. F. Xie, C. Z. Diao, S. B. Xi, B. B. Xiao, C. Hu and W. Y. Choi, *Nat. Commun.*, 2021, **12**.
15. Z. Wei, M. Liu, Z. Zhang, W. Yao, H. Tan and Y. Zhu, *Energy Environ. Sci.*, 2018, **11**, 2581-2589.
16. Y. Kofuji, Y. Isobe, Y. Shiraishi, H. Sakamoto, S. Ichikawa, S. Tanaka and T. Hirai, *ChemCatChem*, 2018, **10**, 2070-2077.
17. L. Zhai, Z. Xie, C.-X. Cui, X. Yang, Q. Xu, X. Ke, M. Liu, L.-B. Qu, X. Chen and L. Mi, *Chem. Mater.*, 2022, **34**, 5232-5240.
18. C. Krishnaraj, H. Sekhar Jena, L. Bourda, A. Laemont, P. Pachfule, J. Roeser, C. V. Chandran, S. Borgmans, S. M. J. Rogge, K. Leus, C. V. Stevens, J. A. Martens, V. Van Speybroeck, E. Breynaert, A. Thomas and P. Van Der Voort, *Journal of the American Chemical Society*, 2020, **142**, 20107-20116.
19. Q. Zhi, W. Liu, R. Jiang, X. Zhan, Y. Jin, X. Chen, X. Yang, K. Wang, W. Cao, D. Qi and J. Jiang, *Journal of the American Chemical Society*, 2022, DOI: 10.1021/jacs.2c09482.
20. H. Kim, K. Shim, K. E. Lee, J. W. Han, Y. Zhu and W. Choi, *Appl. Catal. B*, 2021, **299**, 120666.
21. M. Kou, Y. Wang, Y. Xu, L. Ye, Y. Huang, B. Jia, H. Li, J. Ren, Y. Deng, J. Chen, Y. Zhou, K. Lei, L. Wang, W. Liu, H. Huang and T. Ma, *Angew. Chem. Int. Ed.*, 2022, **61**, e202200413.

22. Y. Shiraishi, T. Takii, T. Hagi, S. Mori, Y. Kofuji, Y. Kitagawa, S. Tanaka, S. Ichikawa and T. Hirai, *Nat. Mater.*, 2019, **18**, 985-993.

23. H. B. Vibbert, C. Bendel, J. R. Norton and A. J. Moment, *Acs. Sustain. Chem. Eng.*, 2022, **10**, 11106-11116.

24. Y. Isaka, Y. Kawase, Y. Kuwahara, K. Mori and H. Yamashita, *Angew. Chem. Int. Ed.*, 2019, **58**, 5402-5406.

25. M. J. Pavan, H. Fridman, G. Segalovich, A. I. Shames, N. G. Lemcoff and T. Mokari, *ChemCatChem*, 2018, **10**, 2541-2545.

26. R. Arcas, E. Peris, E. Mas-Marza and F. Fabregat-Santiago, *Sustain. Energy Fuels*, 2021, **5**, 956-962.

27. I. Krivtsov, A. Vazirani, D. Mitoraj and R. Beranek, *ChemCatChem*, DOI: 10.1002/cctc.202201215.